1521-0103/384/3/429–438$35.00
THE JOURNAL OF PHARMACOLOGY AND EXPERIMENTAL THERAPEUTICS

dx.doi.org/10.1124/jpet.122.001401
J Pharmacol Exp Ther 384:429–438, March 2023

The Journal of PHARMACOLOGY And Experimental Therapeutics

Disruption of Ovarian Cancer STAT3 and p38 Signaling with a Small-Molecule Inhibitor of PTP4A3 Phosphatase[S]

John S. Lazo, Kelly N. Isbell, Sai Ashish Vasa, Danielle C. Llaneza, Ettore J. Rastelli, Peter Wipf, and Elizabeth R. Sharlow

Department of Pharmacology, University of Virginia, Charlottesville, Virginia (J.S.L., D.C.L., E.R.S.); KeViRx, Inc., Charlottesville, Virginia (J.S.L., K.N.I., S.A.V., E.R.S.); and Department of Chemistry, University of Pittsburgh, Pittsburgh, Pennsylvania (E.J.R., P.W.)

Received August 5, 2022; accepted December 19, 2022

ABSTRACT

Protein tyrosine phosphatase type IVA member 3 (PTP4A3 or PRL-3) is a nonreceptor, oncogenic, dual-specificity phosphatase that is highly expressed in many human tumors, including ovarian cancer, and is associated with a poor patient prognosis. Recent studies suggest that PTP4A3 directly dephosphorylates SHP-2 phosphatase as part of a STAT3-PTP4A3 feedforward loop and directly dephosphorylates p38 kinase. The goal of the current study was to examine the effect of a PTP4A phosphatase inhibitor, 7-imino-2-phenylthieno[3,2-*c*] pyridine-4,6(5*H*,7*H*)-dione (JMS-053), on ovarian cancer STAT3, SHP-2, and p38 kinase phosphorylation. JMS-053 caused a concentration- and time-dependent decrease in the activated form of STAT3, Y^{705} phospho-STAT3, in ovarian cancer cells treated in vitro. In contrast, the phosphorylation status of two previously described direct PTP4A3 substrates, SHP-2 phosphatase and p38 kinase, were rapidly increased with JMS-053 treatment. We generated A2780 and OVCAR4 ovarian cancer cells resistant to JMS-053, and the resulting cells were not crossresistant to paclitaxel, cisplatin, or teniposide. JMS-053–resistant A2780 and OVCAR4 cells exhibited a 95% and 50% decrease in basal Y^{705} phospho-STAT3, respectively. JMS-053–resistant OVCAR4 cells had an attenuated phosphorylation and migratory response to acute exposure to JMS-053. These results support a regulatory role for PTP4A phosphatase in ovarian cancer cell STAT3 and p38 signaling circuits.

SIGNIFICANCE STATEMENT

This study demonstrates that chemical inhibition of PTP4A phosphatase activity with JMS-053 decreases STAT3 activation and increases SHP-2 phosphatase and p38 kinase phosphorylation activation in ovarian cancer cells. The newly developed JMS-053–resistant ovarian cancer cells should provide useful tools to further probe the role of PTP4A phosphatase in ovarian cancer cell survival and cell signaling.

Introduction

The protein tyrosine phosphatases of regenerating liver oncoprotein(PTP4A3 or PRL-3) is one of the most oncogenic known protein tyrosine phosphatases, promoting tumor formation, cell survival, migration, metabolism, and angiogenesis (Yu and Zhang, 2017; Lazo et al., 2021). It is significantly upregulated in more than 75% of all human tumors (Thura et al., 2019), most notably ovarian cancer (OvCa) (Polato et al., 2005; McQueeney et al., 2017; Lazo et al., 2021). Drug resistance and tumor recurrence remain serious problems for patients with OvCa, which represents multiple histologically and genetically distinct subtypes that, unlike some other tumor types, have generally not responded well to molecularly targeted drugs. Nevertheless, OvCa clearly is driven by the dysregulation of intracellular signaling networks, and targeting protein tyrosine phosphatases might, therefore, offer a novel medicinal strategy worth pursuing for a disease with a critical need for more effective treatments.

In patients with the most lethal form of OvCa, high-grade serous OvCa, we (McQueeney et al., 2018) and others (Polato et al., 2005; Ren et al., 2009; Liu et al., 2013) found a strong correlation between high PTP4A3 expression and poor patient survival. PTP4A3 is highly expressed in OvCa, which is likely due to the frequent amplification of chromosome 8q24, where the *ptp4a* gene is located, and the high levels of STAT3, which

The work was supported by grants from National Institutes of Health National Cancer Institute [Grant R43-CA2288775] (to J.S.L. and E.R.S.) and [Grant P30-CA044579] (to J.S.L.), National Heart, Lung, and Blood Institute [Grant R43-HL158409] (to J.S.L.), and Office of Research Infrastructure Programs [Grant S10-OD021723] (to J.S.L.); the Virginia Innovation Partnership Corporation [CCF22-0064-PS] (to J.S.L.); the Fiske Drug Discovery Fund (to J.S.L.); the Cure Alzheimer's Fund (to J.S.L. and E.R.S.); and the Rick Sharp Foundation (to J.S.L.)

J.S.L., P.W., and E.R.S. are coinventors of US Patent No. 10,308,663, which describes the chemical synthesis, composition of matter, and use of JMS-053 for the treatment of cancer. J.S.L., P.W., and E.S. are cofounders of KeViRx, Inc, which has an option to license the above-mentioned intellectual property from the University of Virginia and University of Pittsburgh. K.N.I. and S.A.V. were or are employees of KeViRx, Inc.

dx.doi.org/10.1124/jpet.122.001401.

[S] This article has supplemental material available at jpet.aspetjournals.org.

ABBREVIATIONS: A2780 RES, JMS-053-resistant cells; A2780 WT, A2780 wild-type; FBS, fetal bovine serum; IL-6, interleukin-6; JMS-053, 7-imino-2-phenylthieno[3, 2-*c*]pyridine-4, 6(5*H*, 7*H*)-dione; MAPK, mitogen activated protein kinase; OvCa, ovarian cancer; OVCAR4 RES, JMS-053–resistant OVCAR4 cells; OVCAR4 WT, OVCAR4 wild-type; PTP4A3 or PRL-3, protein tyrosine phosphatase of regenerating liver 3; STAT3, signal transducer and activator of transcription 3; TBS-t, Tris-buffered saline with Tween 20.

is a PTP4A3 transcriptional activator (McQueeney et al., 2017; Chong et al., 2019). PTP4A3 controls the phosphorylation status of a remarkable number of intracellular signaling proteins, which alters transcription, receptor signaling dynamics, and cytokine release (Aguilar-Sopena et al., 2020), although its direct substrates have not been firmly established. One study (Chong et al., 2019) demonstrated PTP4A3 participates with signal transducer and activator of transcription 3 (STAT3) in a feedforward loop with SHP-2 phosphatase (also known as PTPN11) in multiple myeloma. Increased intracellular PTP4A3 causes a biphasic activation of STAT3 by Y^{705} phosphorylation, which is mediated through the direct interaction and dephosphorylation of SHP-2 phosphatase by PTP4A3 (Chong et al., 2019). More recently, PTP4A3 has been reported to directly dephosphorylate and inactivate p38 mitogen-activated protein kinase (MAPK) (Shi et al., 2021). STAT3, SHP-2, and p38 regulate many processes involved in cancer. Activated STAT3 is highly expressed in OvCa and associated with poor patient survival (Wu et al., 2019). Downregulation of STAT3 mitigates the malignant behavior of cancer cells (Wu et al., 2019). Currently, the role of activated p38 MAPK is controversial, with some reports indicating it contributes to cancer cell drug resistance, migration, and invasion, whereas others suggest it is a tumor suppressor with a role in regulating cell death processes (Wagner and Nebreda, 2009; Yue and López, 2020; Shi et al., 2021). This may reflect the involvement of multiple isoforms of p38 kinase.

We previously described the design and synthesis of the potent, allosteric, small-molecule PTP4A3 inhibitor, 7-imino-2-phenylthieno[3,2-*c*]pyridine-4,6(5*H*,7*H*)-dione (also known as JMS-053 or KVX-053) (Salamoun et al., 2016; Tasker et al., 2019) and demonstrated in vitro cytotoxicity against multiple chemosensitive and chemoresistant human OvCa cell lines (McQueeney et al., 2017; Lazo et al., 2021). Importantly, no significant cell death was observed with normal IMR-90 fibroblast and ovarian surface epithelial cells. Additionally, we documented that JMS-053 reduced the dissemination of human drug-resistant OvCa in mice (Lazo et al., 2021). In vitro studies demonstrated that JMS-053 had considerable specificity for the PTP4A family of phosphatases, namely PTP4A1, PTP4A2, and PTP4A3, but did not inhibit a panel of 23 other phosphatases nor 49 protein kinases (McQueeney et al., 2017). In the current study, we created and evaluated two OvCa cell lines with acquired resistance to JMS-053 in vitro. Our study was motivated by the long history of using drug-resistant cell lines to provide valuable mechanistic information about new anticancer agents (Johnson et al., 1993; Gottesman, 2002).

Materials and Methods

Cells and Reagents. A2780 cells were purchased from the American Type Culture Collection (Manassas, VA). OVCAR4 cells were purchased from Charles River (Frederick, MD). All OvCa cell lines were cultured in RPMI 1640 medium without any penicillin or streptomycin antibiotics but supplemented with 10% FBS, and all OvCa cell lines were used within 20 passages from stocks unless otherwise noted and were routinely tested for mycoplasma contamination. The syntheses and chemical characterization of JMS-053 and its analog EJR-876-35 have previously been described (Salamoun et al., 2016; Tasker et al., 2019; Rastelli et al., 2020), as has the analog EJR-876-35 (Rastelli et al., 2021). We used our synthesized compound for some experiments as well as JMS-053 purchased from AOBIOUS, Inc (Gloucester, MA) for other studies without obvious differences. The source for the antibodies and other reagents used in our studies are found in Supplemental Table 1. Unless otherwise noted, all other reagents were purchased from ThermoFisher Scientific-Invitrogen (Carlsbad, CA).

We initially selected the well characterized A2780 and OVCAR4 cells to study JMS-053 resistance because they represent BRCA1/2 wild-type, homologous recombination proficient human cell lines with either wild-type TP53 (A2780) or mutant TP53 (Leu130Val) (OVCAR4). Most high-grade serous OvCa, as represented by OVCAR4, either have mutant or deleted TP53, which confers drug resistance. A2780 and OVCAR4 wild-type and resistant cells were harvested at 1.6–6.0 × 10^5 cells/cm^2. A2780 cells were split 1:15 twice weekly, and OVCAR4 cells were split 1:10 approximately once a week. Our initial attempt to develop a compound-resistant cell line was based on a modified Fibonacci concentration escalation model with observational changes included to ensure the development of resistant cell lines. Initially, A2780 and OVCAR4 cells were exposed continuously to 10 μM JMS-053, which resulted in death and detachment from the monolayer of all of the cells within 3 days. We, therefore, modified our exposure procedure with an initial exposure to 5 μM JMS-053. Because we observed considerable cell death 3 days after exposure to 5 μM JMS-053, we removed half of the medium from the A2780 and OVCAR4 cells and replaced it with compound-free medium and 10% FBS to yield a final concentration of 2.5 μM followed 3 days later by a further decrease in the JMS-053 concentration to 1 μM. We had several concentration-escalation schemes, but, surprisingly, only one complex scheme was successful for A2780 cells and resulted in a resistant population (Supplemental Fig. 1). We grew the A2780 cells in 1 μM of JMS-053 for 22 days and then provided the cells with a compound-free holiday for 9 days. The resulting A2780 cells were exposed to 1 μM JMS-053 for 16 days and then grown in JMS-053 at 2 μM for 7 days, 4 μM for 12 days, 8 μM for 6 days, 16 μM for 4 days, 30 μM for 5 days, and 40 μM for 5 days, at which time the A2780 cells resistant to JMS-053 (A2780 RES cells) were frozen until further use. For OVCAR4 cells, we took the above-mentioned cells growing in 1 μM JMS-053 and placed them in compound-free medium and 10% FBS for 14 days. The resulting OVCAR4 cells were then grown in JMS-053 at 3 μM for 7 days, 12 μM for 7 days, 20 μM for 10 days, 10 μM for 14 days, 5 μM for 12 days, 10 μM for 19 days, 20 μM for 6 days, and 40 μM for 21 days, at which time the OVCAR cells resistant to JMS-053 (OVCAR4 RES cells) were frozen until further use. A schematic of our resistance procedures for A2780 RES and OVCAR4 RES cells can be found in Supplemental Fig. 1.

Cell Proliferation and Viability Assays. To generate the cellular growth curves, we plated 6 × 10^5 A2780 cells or 6.5 × 10^5 OVCAR4 cells in T-25 cm^2 tissue culture flasks and counted the resident cell number at various times after incubation (37°C, 5% CO_2) via hemocytometer ($N = 4$). Nonviable cells were stained with Trypan blue (MP Biomedicals) and eliminated from the total cell count. For the compound effects on A2780 and OVCAR4 cell viability, we used a resazurin-based CellTiter Blue (Promega, Fitchburg, WI) assay. All OvCa cell lines were cultured in complete growth medium, with 500 cells/22 μL being seeded into each well of a 384-well black/clear microtiter plate (Greiner Bio-One, VWR, Radnor, PA). If a compound was being tested, it was added (3 μL) at the time the cells were seeded. Cisplatin and carboplatin were resuspended in PBS, and all other compounds were solubilized in DMSO. The final concentration of either PBS or DMSO (0.5%) was matched as the vehicle control concentration. The positive control wells had a final concentration of 10% DMSO. The microtiter plates were incubated for 48 hours (37°C, 5% CO_2), at which time 5 μL of the resazurin-based CellTiter Blue reagent were added. Following an additional 4 hours of incubation (37°C, 5% CO_2), data were captured on a TECAN GENios Pro plate reader with a $A535_{EX}/A590_{EM}$. EC_{50} values were calculated using GraphPad Prism 9.3.0 software (San Diego, CA, USA).

Colony Formation Assays. OvCa cells were seeded at 100 cells per well in 6-well tissue culture plates and incubated (37°C, 5% CO_2) for 10 days. Cells were fixed in 10% acetic acid and 10% ethanol, then

stained in 1% Crystal Violet. Colonies of ~50 cells or more were counted manually.

Cell Migration Assay. OVCAR4 WT or OVCAR4 RES cells were seeded at 2.5×10^5 cells per well in 6-well plates and allowed to adhere at a confluent state for 24 hours when the medium was removed and replaced with fresh RPMI medium containing 2% FBS. Cells were incubated overnight and scratched longitudinally and horizontally with a P1000 pipette tip. The medium and any nonadherent cells were removed, and fresh vehicle control or JMS-053 (4.5 μM)-containing RPMI medium with 15 ng/mL interleukin-6 (IL-6) and 2% FBS was added. Cell migration was determined at 0 hours and 24 hours later by microscopic imaging captured using DinoScope software (version 2.0, Dino-Lite, Torrance, CA), and the cell-free area at the site of the scratch was quantified using ImageJ software.

Western Blot Analysis. Cells and tissues were lysed in M-PER supplemented with 1x Phosphatase and Protease Inhibitor Cocktail. Lysates were sonicated, then centrifuged for 15 minutes at 14,000*g* at 4°C. Protein concentrations were determined with the Pierce Detergent Compatible Bradford Assay Reagent protein assay. Proteins (5–30 μg) were separated with Novex NuPAGE reagents and transferred to nitrocellulose membranes. Membranes were blocked in 5% nonfat milk in Tris-buffered saline with Tween 20 (TBS-t) for 1 hour, then incubated in primary antibodies (1:500–1:2000 dilutions in 5% bovine serum albumin in TBS-t) overnight at 4°C. Membranes were washed in TBS-t, then incubated with secondary antibodies (1:10,000 dilution in 5% bovine serum albumin in TBS-t) for 1 hour at room temperature. Membranes were washed in TBS-t and TBS, then imaged with a LI-COR Odyssey. Band intensities were quantified with Image Studio Ver 5.2 and normalized to glyceraldehyde-3-phosphate dehydrogenase expression.

Real-Time Quantitative Polymerase Chain Reaction. Total RNA was extracted from OvCa cells using an RNAeasy Plus Mini Kit (Qiagen) per the manufacturer's protocol. RNA (4 μg) was converted to cDNA with the RT^2 Easy First Strand (Qiagen). Primers were obtained from Qiagen. Real-time monitoring of the quantitative polymerase chain reaction was performed on a BioRad CFX Connect with RT^2 SYBR Green qPCR Mastermix (Qiagen). The reaction was incubated at 95°C for 10 minutes, then run for 40 cycles at 95°C for 15 seconds and 60°C for 1 minute. PTP4A1-3 gene expression was normalized to human glyceraldehyde-3-phosphate dehydrogenase expression.

Statistical Analyses. Data were analyzed using ANOVA and Wilcoxon *t* test with GraphPad Prism 9.3 Software unless indicated otherwise. Statistical significance was determined as described in the text.

Results

Growth Rates, Resistance Profiles, and Cloning Efficiency of JMS-053–Resistant OvCa Cells. We found the generation of resistance to JMS-053 challenging, with almost complete cell death of A2780 and OVCAR4 cells after an initial exposure of cells to a concentration of 10 μM JMS-053. Therefore, we decreased the initial exposure concentration of JMS-053 to 5 μM and 1 μM for A2780 and OVCAR4 cells, respectively, and completed the acquired resistance protocol described in *Materials and Methods* and outlined in Supplemental Fig. 1. We isolated A2780 and OVCAR4 cells that were 33-fold and fourfold more resistant to JMS-053 than their isogenic wild-type parental lines, respectively (Fig. 1, A and B). Interestingly, in the absence of JMS-053, we detected no significant difference in the in vitro growth rate of A2780 wild-type (A2780 WT) [23.1 ± 4.1 hours, (S.D.), $N = 4$], which is in agreement with the literature (Behrens et al., 1987), and the JMS-053–resistant cells (A2780 RES) [doubling time = 24.8 ± 0.7 hours, (S.D.), $N = 4$] (Fig. 2A). The A2780 WT cells had an IC_{50} for JMS-053 of 522 nM, whereas the 33-fold resistant A2780 RES cells had an IC_{50} value of 17.0 μM (Fig. 2A; Table 1; Supplemental Fig. 2A). The A2780 RES population was stable in the absence of JMS-053 exposure for at least 24 days (Fig. 1C). The A2780 RES cells showed no evidence of crossresistance to the current OvCa standard-of-care drugs: paclitaxel, carboplatin, or cisplatin (Table 1; Supplemental Fig. 2, B–D). Moreover, we observed no crossresistance to teniposide and a very slight sensitization to idarubicin (Table 1; Supplemental Fig. 1, E and F). A2780 RES cells were threefold crossresistant to the previously described (Rastelli et al., 2021) JMS-053 analog, EJR-876-35, compared with the A2780 WT cells (Table 1).

We found the generation of OVCAR4 cell resistance to JMS-053 required a longer exposure time to JMS-053 than with A2780 cells (Supplemental Fig. 1), which might reflect the slower proliferation rate of the OVCAR4 cells compared with the A2780 cells. No significant difference was detected in the growth rates of the OVCAR4 wild-type (OVCAR4 WT) [49.6 ± 4.5 hours, (S.D.), $N = 4$], which agrees with the literature (Cowley et al., 2014), and the resulting JMS-053–resistant OVCAR4 cells (OVCAR4 RES) [43.0 ± 7.0 hours, (S.D.),

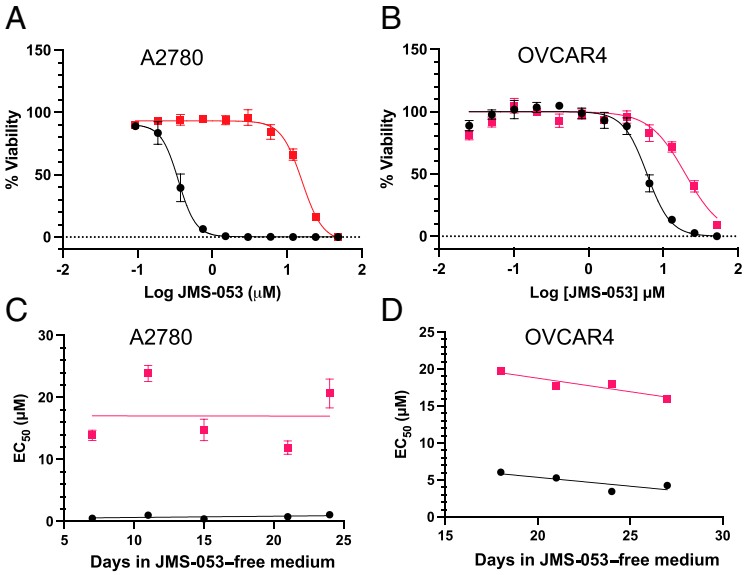

Fig. 1. Generation of durable JMS-053–resistant A2780 and OVCAR4 cells. (A) A2780 cells with 33-fold resistance to a 72-hour exposure to JMS-053 compared with wild-type A2780 cells. Viability determined by hemocytometer after incubation with Trypan blue. Black circles indicate A2780 WT, and red squares indicates JMS-053–resistant cells (A2780 RES). $N = 3$; bar = S.D. unless smaller than the symbol. (B) OVCAR4 cells with fourfold resistance to a 72-hour exposure to JMS-053 (OVCAR4 RES) compared with OVCAR4 WT cells. Viability determined by hemocytometer after incubation with Trypan blue. Black circles indicate OVCAR4 WT cells, and red squares indicates OVCAR4 RES cells. $N = 3$; bar = S.D. unless smaller than the symbol. (C) Retention of JMS-053 resistance in A2780 RES cells. Each symbol represents the mean value obtained from three technical replicates, and the bars indicate the S.D. unless smaller than the symbol. Black circles indicate A2780 WT cells, and red squares indicate A2780 RES cells. (D) Retention of JMS-053 resistance in OVCAR4 RES cells. Each symbol represents the mean value obtained from three technical replicates, and the bars indicate the S.D. unless smaller than the symbol. Black circles indicate OVCAR4 WT cells, and red squares indicates OVCAR4 RES cells.

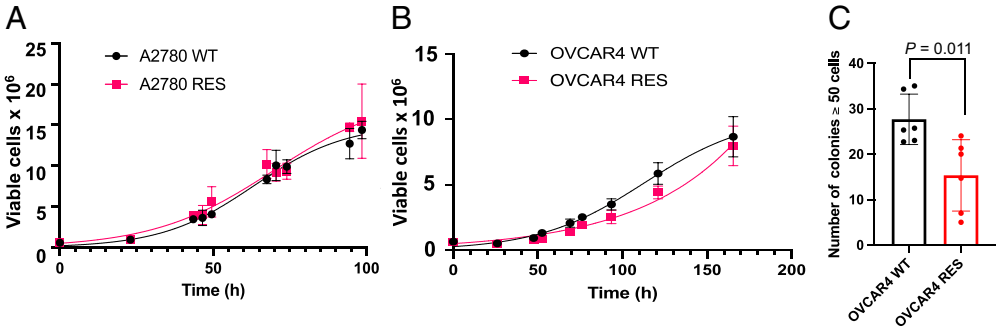

Fig. 2. Growth rates and colony-forming efficacy of JMS-053–resistant OvCa cells. A2780 RES (A) and OVCAR4 RES (B) cells have similar growth rates compared with parental wild-type cells. A2780 cells (6×10^5) and OVCAR4 cells (6.5×10^5) were plated in T-25 cm^2 tissue culture flasks, and cell growth rate was determined by hemocytometer. A2780 WT and OVCAR4 WT are indicated by black circles; A2780 RES and OVCAR4 RES cells are indicated by red rectangles. Bars = S.D. unless smaller than the symbols, $N = 4$. Representative growth curves of three biologic replicates are shown. (C) OVCAR4 RES cells have lower colony-forming efficiency compared with OVCAR4 WT cells. Each symbol represents the mean number of colonies with >50 cells counted 10 days after plating 100 cells from six biologic replicates. Bars = S.D. $P = 0.011$ with unpaired two tailed t test.

$N = 4$] (Fig. 2B). The OVCAR4 RES cells were fourfold resistant to JMS-053, with an IC_{50} value of 17.85 μM compared with an IC_{50} value of 4.76 μM for the wild-type OVCAR4 cells (Fig. 1B; Table 1; Supplemental Fig. 3A). Collectively, these results suggest that the acquired resistance to JMS-053 in the A2780 and OVCAR4 cell lines was not secondary to a slower proliferation rate of the JMS-053–resistant cell population. Moreover, like A2780 RES cells, OVCAR4 RES cells were not crossresistant to paclitaxel, cisplatin, teniposide, or idarubicin (Table 1; Supplemental Fig. 3, B–D). Surprisingly, the OVCAR4 RES cells were slightly more sensitive to EJR-876-35 (Table 1; Supplemental Fig. 3E). Similar to the A2780 RES cell population, the OVCAR4 RES population exhibited stable JMS-053 resistance in the absence of JMS-053 exposure for at least 3 weeks (Fig. 1D). Although we detected no significant difference in the growth rates of the wild-type and resistant OVCAR4 populations grown on plastic, we did observe a 45% decrease in the colony-forming efficiency of the OVCAR4 RES compared with OVCAR4 WT (Fig. 2C), suggesting potential alterations in intracellular signaling pathways in these OvCa cells induced by chronic exposure to JMS-053.

PTP4A3 Expression in JMS-053–Resistant Cells. We next examined the basal mRNA and protein levels of PTP4A3 in the cells with acquired resistance because it is known that altered molecular target levels sometimes are seen in resistant cells. Similar PTP4A3 mRNA expression levels were seen, however, when A2780 RES cells were directly compared with A2780 WT cells (Fig. 3A) and when OVCAR4 RES cells were directly compared with the OVCAR4 WT cells (Fig. 3B). PTP4A1 mRNA levels also were not different when directly comparing the wild-type and resistant cells (Fig. 3, A and B). Although a few of the resistant cell lysates appeared to have elevated PTP4A2 mRNA levels, most lysates were not markedly increased compared with those from wild-type cells. PTP4A3 western blot analyses of protein lysate indicated that A2780 cells had higher protein expression than OVCAR4 cells, but we found no evidence for altered PTP4A3 protein levels in wild-type and resistant cells (Fig. 3, C and D, Supplemental Fig. 5).

Differences in STAT3 and p38 Kinase Phosphorylation With the Resistant Cell Populations. Because of the central role STAT3 activation has in OvCa malignancy (Wu et al., 2019), we determined the basal phosphorylation status of the two epitopes involved in STAT3 activation, Y^{705} and S^{727}, in the A2780 cell wild-type and resistant pairs. In A2780 RES cells, we observed a 95% and 40% decrease in phospho-Y^{705} and phospho-S^{727} STAT3, respectively, with no difference in total STAT3 protein levels (Fig. 4, A and B). In OVCAR4 RES cells, phospho-Y^{705} STAT3 phosphorylation was 50% less than in OVCAR4 WT cells, whereas the phospho-S^{727} STAT3 and STAT3 protein levels were similar (Fig. 4, C and D). We focused the remainder of our attention on potential differences in the intracellular signaling pathways in the OVCAR4 cell population for several reasons. First, because unlike A2780 cells, OVCAR4 cells are a well accepted model of high-grade serous OvCa, which is the most lethal form of the disease and is generally intrinsically drug resistant (Lengyel, 2010; Cowley et al., 2014; Lazo et al., 2021). Second, unlike A2780 cells, OVCAR4 cells have a mutated nonfunctional TP53 and, thus, represent the vast majority of high-grade serous OvCa. Third, we found that OVCAR4 cells were one of the most sensitive high-grade serous OvCa cell lines to JMS-053 in our previous study (Lazo et al., 2019). Fourth, we observed a decrease in the OVCAR4 RES colony-forming ability compared with OVCAR4 WT cells (Fig. 2C). Fifth, OVCAR4 had previously been reported to basally secrete among the highest amounts of IL-6 in the OvCa cells that were surveyed (Wang et al., 2018).

Acute Exposure to JMS-053 Alters the Phosphorylation Status of STAT3, SHP-2, and p38 Kinase. We next examined the effects of an acute exposure of OVCAR4 WT cells to JMS-053. We selected acute concentrations that we

TABLE 1
Sensitivity of A2780 cells with acquired JMS-053 resistance to other drugs

	μM ± S.D. (N)						
A2780	JSM-053	Paclitaxel	Idarubicin	Carboplatin	Cisplatin	Teniposide	EJR-876-35
Wild-Type	0.522 ± 0.251 (9)	0.0029 ± 0.0012 (5)	10.907 ± 1.199 (4)	80.312 ± 26.748 (4)	7.260 (1)	82.489 ± 40.106 (7)	5.178 ± 0.976 (4)
Resistant	17.031 ± 3.605 (9)*	0.0023 ± 0.0010 (5)	7.376 ± 0.001 (4)**	83.217 ± 19.930 (4)	5.124 (1)	53.412 ± 19.930 (7)	15.133 ± 5.965 (4)***

*$P < 0.003$; ** $P = 0.009$; *** $P = 0.028$.

TABLE 2
Sensitivity of OVCAR4 cells with acquired JMS-053 resistance to other other drugs
Cells were treated with compounds continuously for 72 hours, and the IC50 values were determined from the biological replicates indicated in parentheses.

	μM ± S.D. (N)					
OVCAR4	JMS-053	Paclitaxel	Idarubicin	Cisplatin	Teniposide	EJR-876-35
Wild-Type	4.76 ± 0.99 (4)	0.0148 ± 0.0116 (4)	0.369 (1)	4.56 ± 2.60 (4)	3.99 ± 1.83 (4)	18.41 ± 2.28 (3)
Resistant	17.85 ± 1.33 (4)*	0.0089 ± 0.0064 (4)	0.351 (1)	3.44 ± 1.82 (4)	5.87 ± 2.46 (4)	11.30 ± 2.90 (3)**

*P = 0.0003; **P = 0.05.

previously determined (Fig. 1) caused a 25% (1.5 μM), 50% (4.5 μM), and 90% (40 μM) decrease in cell survival when OVCAR4 WT cells were exposed continuously for 72 hours to JMS-053. We observed a marked decrease in Y^{705} STAT3 phosphorylation, which indicated inactivation, within 1 hour with 4.5 μM and 40 μM JMS-053 that lasted 4 or 6 hours, respectively (Fig. 5, A and B, Supplemental Fig. 6). OVCAR4 cells exposed to 1.5 μM displayed a modest increase in Y^{705} STAT3 phosphorylation only at 4 hours (Fig. 5, A and B, Supplemental Fig. 6). The phosphorylation status of S^{727} was decreased with 40 μM JMS-053 exposure after a 2-hour exposure and was maintained for at least 6 hours (Fig. 5, A and C).

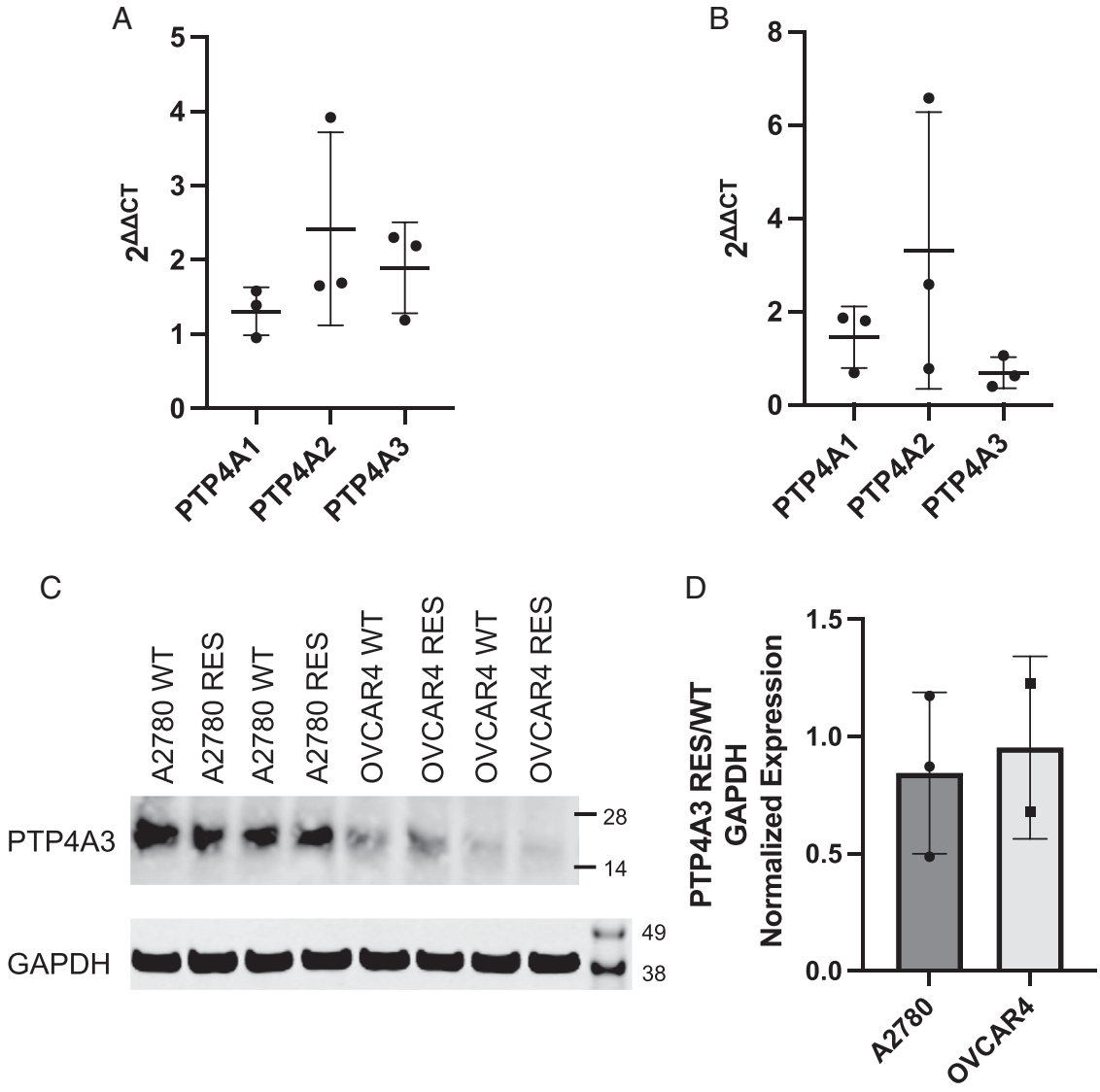

Fig. 3. JMS-053–resistant cells do not have markedly altered PTP4A3 expression levels. (A) Differences in the PTP4A1-3 mRNA levels in A2780 WT and A2780 RES cells determined by reverse-transcription polymerase chain reaction (RT-PCR) from three technical replicates. Bars = S.D. (B) Differences in the PTP4A1-3 mRNA levels in OVCAR4 WT and OVCAR4 RES cells determined by RT-PCR from three technical replicates. Bars = S.D. (C) Western blots for PTP4A3 protein with lysates from A2780 and OVCAR4 cells. (D) Ratio of the PTP4A3 protein levels in wild-type and JMS-053–resistant A2780 and OVCAR4 cells as determined by western blotting and normalized to the glyceraldehyde-3-phosphate dehydrogenase (GAPDH) loading control. Each symbol indicates the mean value from a technical replicate, with the bars representing the S.D. or the range from biologic replicates.

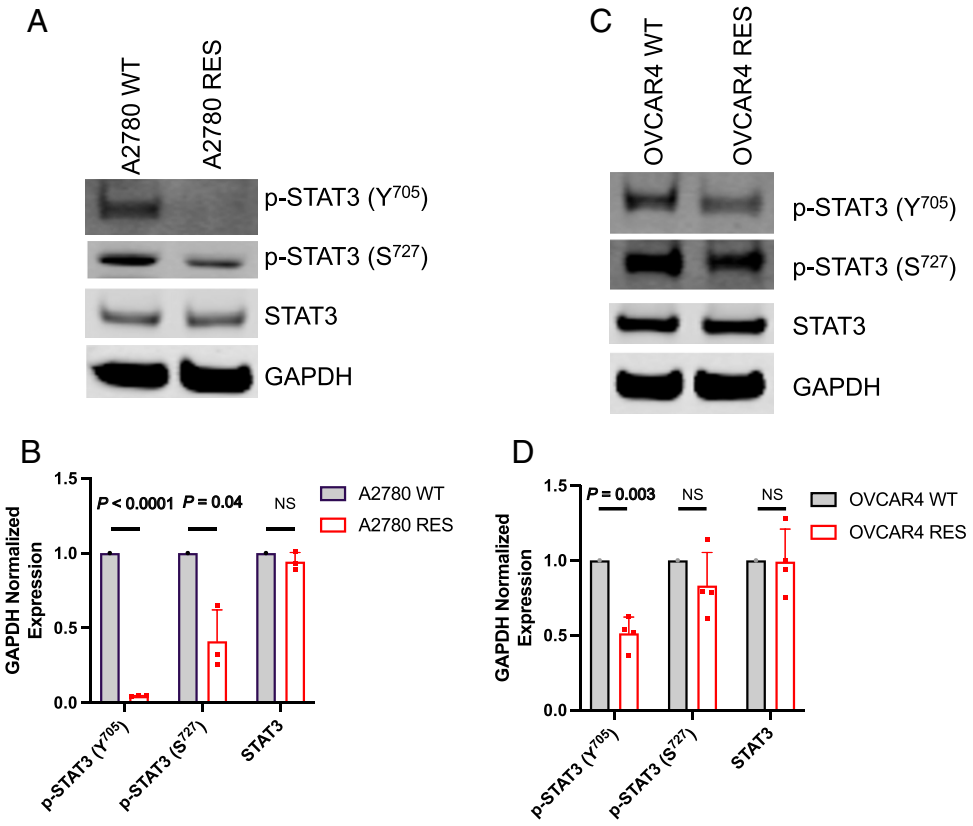

Fig. 4. Cells with acquired resistance to JMS-053 have reduced basal STAT3 phosphorylation and activation levels. (A) Representative western blots of A2780 WT and A2780 RES Y^{705} p-STAT3, S^{727} p-STAT3, STAT3, and glyceraldehyde-3-phosphate dehydrogenase (GAPDH). (B) Quantification of A2780 WT (gray bars) and A2780 RES (red bars) western blot signal normalized to GAPDH. $N = 3$ biologic replicates. Bars = S.D. One-sample two tailed t test with Wilcoxon test. NS = $P > 0.05$. (C) Western blots of A2780 WT and A2780 RES Y^{705} p-STAT3, S^{727} p-STAT3, STAT3 and GAPDH. (D) Quantification of OVCAR4 WT (gray bars) and OVCAR4 RES (red bars) western blot signal normalized to GAPDH. $N = 4$. Bars = S.D. Two-tailed t test with Wilcoxon test. NS, not significant.

Mechanistically, PTP4A3 has previously been shown in multiple myeloma cells to directly bind and dephosphorylate SHP-2 (Chong et al., 2019). Phosphorylated Y^{580} SHP-2 enables gp130-mediated repression of STAT3 phosphorylation and activation (Chong et al., 2019). Consistent with this hypothesis and a role for SHP-2 as a direct substrate for PTP4A3, we observed a marked increase in Y^{580} and Y^{542} SHP-2 phosphorylation within 7 minutes after exposure of OVCAR4 WT cell exposure to JMS-053 (Fig. 6). We found no evidence for a reproducible change in total SHP-2

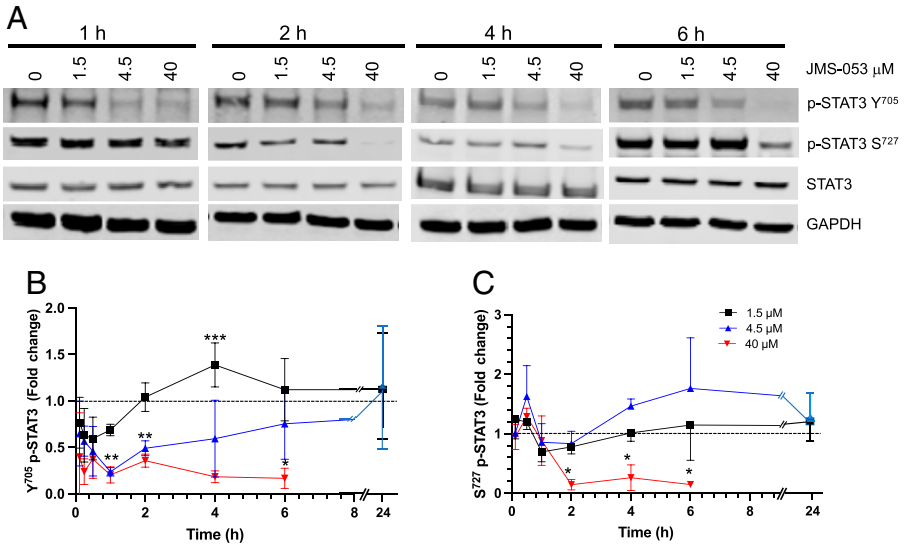

Fig. 5. Acute exposure of OVCAR4 cells to JMS-053 decreases STAT3 activation and phosphorylation. (A) Representative western blots of OVCAR4 WT cell protein lysates after exposure to JMS-053 measuring Y^{705} p-STAT3, S^{727} p-STAT3, STAT3, and glyceraldehyde-3-phosphate dehydrogenase. (B) Kinetics of Y^{705} p-STAT3 changes in OVCAR4 WT cells exposed to different concentrations of JMS-053. $N = 3$ or 4. Bars = S.D. Data analyzed with ANOVA and t test with Wilcoxon test. *$P < 0.05$ for the values found below the asterisk compared with vehicle control. **$P < 0.05$ for the two values found below the asterisks compared with vehicle control. ***$P < 0.05$ for the three values found below the compared with vehicle control. Black dotted line indicates value at 0 hours. (C) Kinetics of S^{727} p-STAT3 changes in OVCAR4 WT cells exposed to different concentrations of JMS-053. Black squares indicate lysates from cells treated with 1.5 μM JMS-053, blue triangles indicate lysates from cells treated with 4.5 μM JMS-053, and red inverted triangles indicate lysates from cells treated with 40 μM JMS-053. $N = 3$ or 4. Bars = S.D. Data analyzed with ANOVA and t test with Wilcoxon test. *$P < 0.05$ for the value found below the asterisk compared with vehicle control. Black dotted line indicates value at 0 hours.

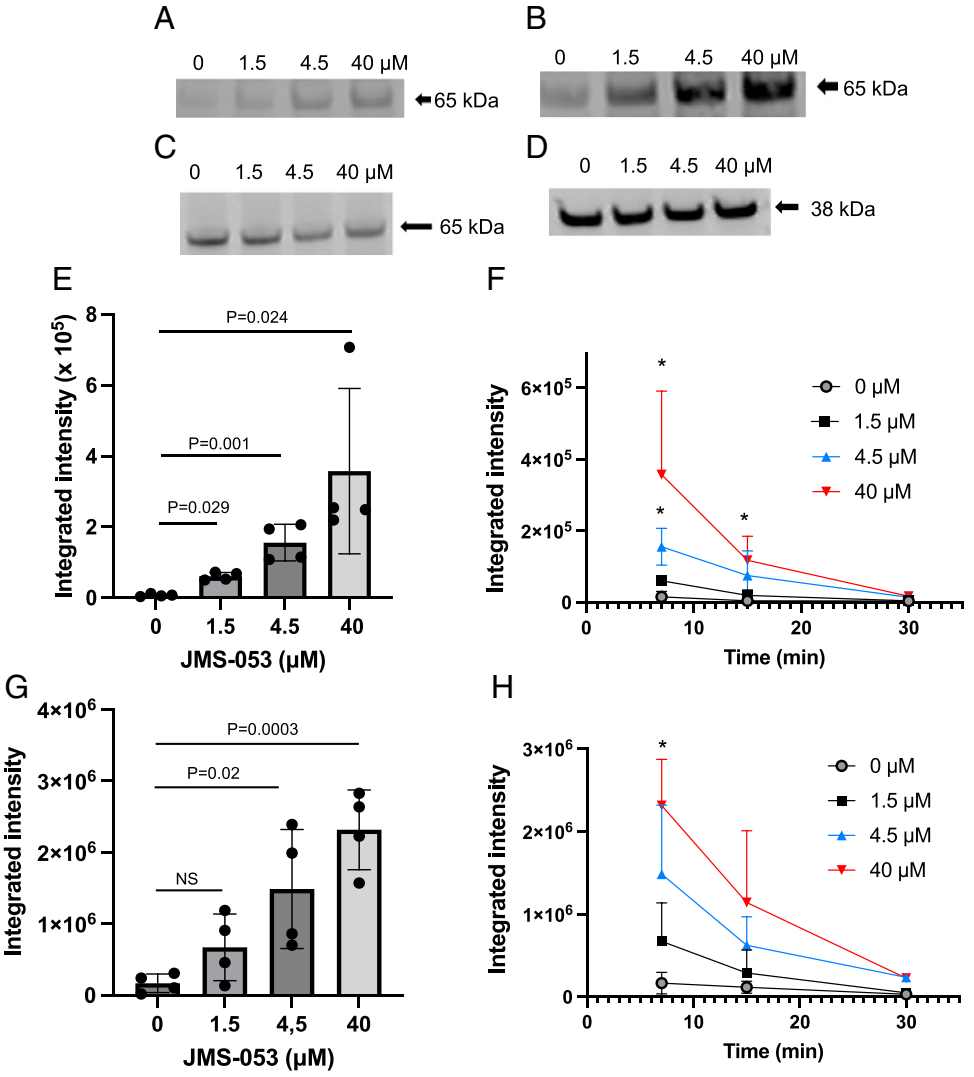

Fig. 6. Acute exposure of OVCAR4 WT cells to JMS-053 rapidly increases Y^{580} and Y^{542} SHP-2 phosphorylation. (A) Representative western blot of OVCAR4 WT cell protein lysates after exposure to JMS-053 for 7 minutes measuring Y^{580} SHP-2 phosphorylation. (B) Representative western blot of OVCAR4 WT cell protein lysates after exposure to JMS-053 for 7 minutes measuring Y^{542} SHP-2 phosphorylation. (C) Representative western blot of OVCAR4 WT cell protein lysates after exposure to JMS-053 for 7 minutes measuring SHP-2 protein levels. (D) Representative western blot of OVCAR4 WT cell protein lysates after exposure to JMS-053 for 7 minutes measuring glyceraldehyde-3-phosphate dehydrogenase (GAPDH). (E) Y^{580} SHP-2 phosphorylation normalized to GAPDH in OVCAR4 WT cell protein lysates after exposure to JMS-053 for 7 minutes. $N = 4$. biologic replicates. Bars = S.D. ANOVA and Mann-Whitney test. (F) Kinetics of Y^{580} SHP-2 phosphorylation normalized to GAPDH in OVCAR4 WT cell protein lysates after exposure to JMS-053. Data analyzed with ANOVA and t test with Wilcoxon test. $^*P < 0.05$ compared with vehicle treated samples. (G) Y^{542} SHP-2 phosphorylation normalized to GAPDH in OVCAR4 WT cell protein lysates after exposure to JMS-053 for 7 minutes. $N = 4$ biologic replicates. Bars = S.D. NS = $P > 0.05$. ANOVA and Mann-Whitney test. (H) Kinetics of Y^{542} SHP-2 phosphorylation normalized to GAPDH in OVCAR4 WT cell protein lysates after exposure to JMS-053. Data analyzed with ANOVA and t test with Wilcoxon test. $^*P < 0.05$ compared with vehicle treated samples.

protein levels (Supplemental Fig. 4A) nor for total STAT5 or Y^{694} STAT5 protein levels (Supplemental Fig. 4, B and C).

Another proposed direct PTP4A3 intracellular substrate is p38 MAPK, which requires phosphorylation at T^{180} and Y^{182} for activation (Shi et al., 2021). Consistent with this hypothesis, JMS-053 caused a rapid concentration-dependent increase in the p38 kinase phosphorylation at T^{180} and Y^{182} (Fig. 7, A and B). Notably, p38 phosphorylation remained elevated for at least 4 hours after exposure to 4.5 μM JMS-053 (Fig. 7, A and B). With 40 μM JMS-053, there was also an increase in p38 phosphorylation within 7 minute that reached fivefold by 15 minutes, with a subsequent decline at 4 hours (Fig. 7, A and B). Collectively, these data supported the engagement of JMS-053 with intracellular PTP4A3.

We next compared the relative changes in the p38 kinase and STAT3 phosphorylation response to JMS-053 by the OVCAR4 WT and OVCAR4 RES cells to probe a possible role of these signaling pathways in the resistance phenotype. In these experiments (Fig. 8), we again observed an increase in p38 activation phosphorylation 30 minutes after exposure of OVCAR4 WT cells to 4.5 and 40 μM JMS-053. After 4 hours of JMS-053 exposure, significant differences were not observed at 1.5 or 4.5 μM, although there was a trend toward a decrease in p38 activation phosphorylation with 40 μM (Fig. 8A). Decreased Y^{705} STAT3 phosphorylation was observed 30 minutes after 1.5, 4.5, and 40 μM JMS-053 exposure and at 4 hours after 40 μM JMS-053 (Fig. 8B). In contrast, OVCAR4 RES p38 kinase phosphorylation and Y^{705} STAT3 phosphorylation were markedly attenuated and were not statistically different from the vehicle control values at either 30 minutes or 4 hours (Fig. 8, C and D). Because of the central role that has been proposed for IL-6 in the STAT3/PTP4A3 feedforward loop (Chong et al., 2019), we predicted that alterations in STAT3 activation would disrupt IL-6–stimulated phenotypic properties of cells. As we have previously demonstrated (Lazo et al., 2021), IL-6 stimulates OvCa cell migration, which is inhibited by JMS-053 (Fig. 8E). In contrast, IL-6–stimulated OVCAR4 RES migration was not inhibited by JMS-053 (Fig. 8E). Collectively, these data are consistent with the hypothesis that alterations in STAT3 and p38 kinase activation participate in the resistance to JMS-053.

Discussion

Unlike many other cancers, OvCa death rates have remained constant, with a 5-year survival rate of <30% for the past 40

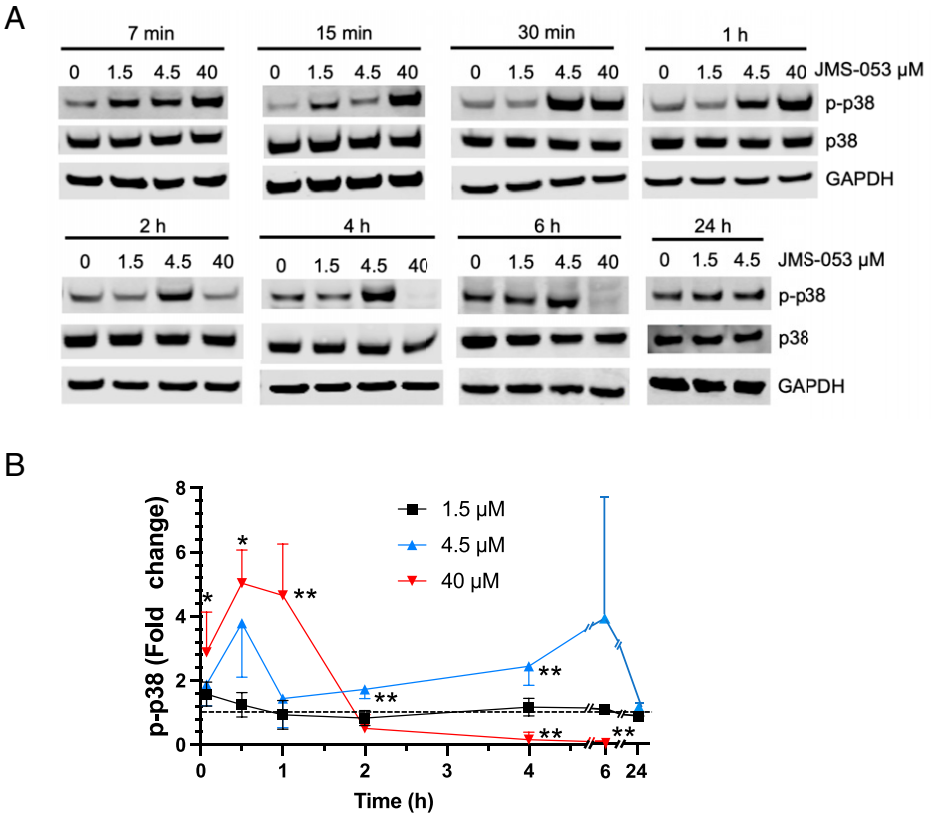

Fig. 7. Acute exposure of OVCAR4 WT cells to JMS-053 increases p38 phosphorylation. (A) Representative western blots of OVCAR4 WT cell protein lysates after exposure to JMS-053 for various times measuring p-p38, p38 kinase, and glyceraldehyde-3-phosphate dehydrogenase (GAPDH). (B) Kinetics of altered p38 phosphorylation by JMS-053 exposure of OVCAR4 WT cells. Fold increase of p-p38, which was normalized to GAPDH, and the corresponding value for lysates from OVCAR4 WT cells exposed to vehicle. Black squares indicate lysates from cells treated with 1.5 μM JMS-053, blue triangles indicate lysates from cells treated with 4.5 μM JMS-053, and red inverted triangles indicate lysates from cells treated with 40 μM JMS-053. N = 3-4. Bars = S.D. Data analyzed with ANOVA and t test with Wilcoxon test. *$P < 0.05$ for the values found below the asterisk compared with vehicle control. **$P < 0.05$ for the individual value found next to the asterisk compared with vehicle control.

years, and high-grade serous OvCa represents ~80% of OvCa, accounting for 67% of all OvCa deaths (Wang et al., 2018). Clearly, there is a need for new approaches to treat this disease. Cells with acquired drug resistance have provided useful and unexpected information about the mechanism of action and resistance of many existing and emerging anticancer agents (Johnson et al., 1993; Gottesman, 2002). Therefore, we established for the first time two human OvCa cell lines with acquired resistance to JMS-053. This compound is valuable because it has in vitro narrow specificity to the three members of the PTP4A family. Our focus on PTP4A3 reflects the observed elevation of PTP4A3 in OvCa, especially in high-grade serous OvCa, compared with PTP4A1 or PTP4A2 (Polato et al., 2005; McQueeney et al., 2017). It should be noted, however, that we cannot exclude an involvement of PTP4A1 or PTP4A2 with JMS-053. Although the majority of reports indicate that increases in PTP4A3 mRNA or protein levels are associated with a poorer overall survival (Polato et al., 2005; Ren et al., 2009; McQueeney et al., 2017), there is at least one publication (Reich et al., 2011) that concluded in a subset of the OvCa patients studied that elevated PTP4A3 mRNA levels were not associated with a decrease overall survival, whereas elevated PTP4A1 and PTP4A2 mRNA levels were associated with a better overall survival. Thus, the role of the PTP4A family in OvCa retains some controversy. The pan-PTP4A inhibitor JMS-053 is potentially useful tool, which, unlike genetic approaches, is titratable and can alter all of the family members simultaneously.

Importantly, the JMS-053–resistant cell lines were not crossresistant to drugs that are currently used in the treatment of OvCa, namely paclitaxel, cisplatin, and carboplatin, consistent with their different mechanisms of action. The JMS-053–resistant cells were also not crossresistant to teniposide or idarubicin, which would suggest that JMS-053 is not exported by ABCB1-like transporters. Surprisingly, the resistant cell lines did demonstrate a reduced ability to generate colonies in vitro in the absence of JMS-053 exposure. In OvCa, loss of colony-forming ability is greatly influenced by the growth factors and cytokines in the microenvironment, and PTP4A3 has been shown to be highly involved in growth factor and cytokine processing and release (Yang et al., 2017; Aguilar-Sopena et al., 2020). Interestingly, we found no marked differences in the PTP4A3 protein levels in the cells with acquired JMS-053 resistance. Although PTP4A3 is rarely mutated in human cancers (McQueeney et al., 2017), we cannot exclude possible mutations nor can we eliminate post-translational differences, such as phosphorylation or lipidation, which are known to influence the phosphatase activity of PTP4A3 (Yu and Zhang, 2017). We also cannot exclude differences in the subcellular localization of PTP4A3. Nonetheless, we did observe marked differences in the basal Y^{705} STAT3 phosphorylation in the cell lines with acquired JMS-053 resistance. Phosphorylation at Y^{705} of STAT3 is essential for its activation and transcriptional activity. Our studies are distinguished from the one previous publication (Chong et al., 2019) that implicates PTP4A3 with STAT3 in a feedforward loop via SHP-2, which focused on IL-6 and multiple myeloma. IL-6 is released by the tumor microenvironment, but it is also known to be secreted by OvCa cells (Nilsson et al., 2005). OVCAR4, in particular, secretes large amounts of IL-6 (Wang et al., 2018). Moreover, we previously demonstrated that PTP4A3 is required for IL-6–stimulated OVCAR4 migration (Lazo et al., 2021). Interestingly, acute exposure to JMS-053 rapidly depleted Y^{705} STAT3, Y^{580} SHP-2, and Y^{542} SHP-2 phosphorylation in OVCAR4 WT

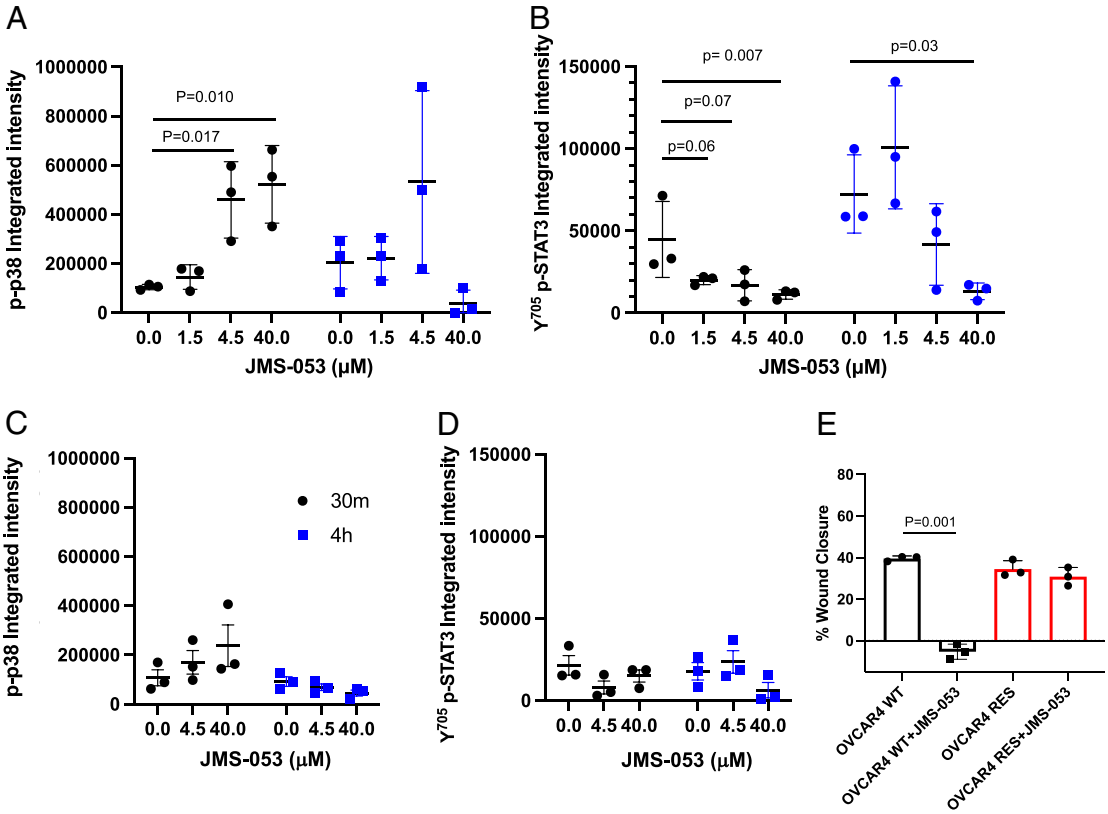

Fig. 8. OVCAR4 RES cells have attenuated phosphorylation responses to JMS-053. (A) OVCAR4 WT cells were treated with various concentrations of JMS-053 for 30 minutes (black circles) or 4 hours (blue squares), and the phosphorylation status of p38 kinase normalized to the glyceraldehyde-3-phosphate dehydrogenase (GAPDH) loading control was determined by western blotting. Bar = S.D. Data analyzed with ANOVA and *t* test with Wilcoxon test. (B) OVCAR4 WT cells were treated with various concentrations of JMS-053 for 30 minutes (black circles) or 4 hours (blue squares), and the phosphorylation status of Y^{705} STAT3 normalized to the GAPDH loading control was determined by western blotting. Data analyzed with ANOVA and *t* test with Wilcoxon test. (C) OVCAR4 RES cells were treated with various concentrations of JMS-053 for 30 minutes (black circles) or 4 hours (blue squares), and the phosphorylation status of p38 kinase normalized to the GAPDH loading control was determined by western blotting. Bars = S.D. Data analyzed with ANOVA and *t* test with Wilcoxon test. (D) OVCAR4 RES cells were treated with various concentrations of JMS-053 for 30 minutes (black circles) or 4 hours (blue squares), and the phosphorylation status of Y^{705} STAT3 normalized to the GAPDH loading control was determined by western blotting. Bars = S.D. Data analyzed with ANOVA and *t* test with Wilcoxon test. (E) Confluent serum-deprived OVCAR4 WT and OVCAR4 RES were uniformly scratch wounded with a pipette and then exposed to 15 ng/mL IL-6 and either vehicle control or JMS-053 (4.5 μM) for 24 hours. Cell migration was calculated by determining the cell-free area at 0 hours and subtracting that from the remaining cell-free area at 24 hours. The data are from three independent biologic replicates and analyzed by *t* test. Bars = S.D.

cells. We previously observed that the STAT3 inhibitor 864,669 inhibited the cytotoxicity of JMS-053 in OvCa cells (Lazo et al., 2021). Thus, our pharmacological studies support the previous conclusion (Chong et al., 2019) that functional STAT3/PTP4A3/SHP-2 loops exist and indicate that the loops also are present in human OvCa cells even when exogenous IL-6 is not added. Moreover, our data support Y^{580} SHP-2 as a direct PTP4A3 intracellular substrate. These observations may explain the large pleotropic signaling effects seen by us and others (Chong et al., 2019) using both pharmacological and genetic tools to change PTP4A3 activity or levels as SHP-2 is known to regulate a wide array of intracellular proteins that are involved in tumor cell colony formation and migration (Chong et al., 2019). The phospho-Y^{580} SHP-2 and Y^{705} phospho-STAT3 changes are likely to be responsible for the marked decrease seen in the colony-forming and migratory ability of OVCAR4 RES cells.

Another prominent pleotropic mammalian cell signal transduction system involves the four conventional MAPK superfamilies, which are extracellular signal-regulated protein kinase 1/2 (ERK1/2), c-Jun N-terminal kinase 1-2 (JNK1-3), p38 kinase, and ERK5. Unlike ERK1/2, which is activated by mitogens and growth factors, physical, chemical, and biologic stress stimuli activate p38 kinase by phosphorylation on T^{180} and Y^{182}. Once activated, p38 kinase phosphorylates a multitude of substrates, including kinases and transcription factors involved in cell survival, migration, and invasion (Shi et al., 2021). The role of p38 kinase in cancer is controversial, however, because some studies have suggested that it acts as a tumor suppressor by regulating apoptosis (Yue and López, 2020; Shi et al., 2021). A recent report implicates p38 kinase as a direct substrate for PTP4A3 in human colorectal, breast, and embryonic kidney cells, especially under stress conditions such as exposure to $CoCl_2$, which produces reactive oxygen species (Shi et al., 2021). The PTP4A3-mediated p38 kinase dephosphorylation was, however, independent of the reactive oxygen species generation (Shi et al., 2021). Interestingly, only PTP4A3 and not PTP4A1 or PTP4A2 dephosphorylates p38 kinase at T^{180} and Y^{182} in vitro (Shi et al., 2021). We previously demonstrated that JMS-053 does not generate reactive oxygen species nor does loss of PTP4A3 produce a gene expression pattern consistent with cellular stress (Lazo et al., 2019). Moreover, we intentionally synthesized bifunctional analogs of JMS-053 capable of inducing cellular stress and found no evidence that exposure of cells to the monofunctional JMS-053 alone caused endoplasmic

stress or the unfolded protein response (Rastelli et al., 2021). Therefore, we believe it is unlikely that the very rapid increase in phosphorylated p38 kinase seen in OVCAR4 in response to JMS-053 exposure is the result of indirect cell stress; rather, it is more likely due to a direct loss of PTP4A3 phosphatase activity. It should be noted, however, that there are multiple isoforms of p38 kinase, and the antibodies we used do not distinguish among them, so additional studies are needed to focus on the role of p38 kinase in the proposed axis. Nevertheless, our study suggests that JMS-053 resistance is the result of alterations in the acute responsiveness of STAT3 and p38 pathways to the compound.

The newly developed JMS-053–resistant cells should be useful tools to further probe the role of PTP4A3 in OvCa cell survival and cell signaling. The involvement of PTP4A3 in the STAT3, SHP-2, and p38 kinase pathways could explain the rather major cancer-relevant changes seen when the PTP4A3 phosphatase levels are altered in human cancers.

Authorship Contributions

Participated in the research design: Lazo, Wipf, Sharlow.

Conducted experiments: Lazo, Isbell, Vasa, Llaneza, Sharlow.

Contributed new reagents or analytical tools: Lazo, Rastelli, Wipf.

Performed data analysis: Lazo, Isbell, Vasa, Llaneza, Sharlow.

Wrote or contributed to the writing of the manuscript: Lazo, Wipf, Sharlow.

References

Aguilar-Sopeña O, Hernández-Pérez S, Alegre-Gómez S, Castro-Sánchez P, Iglesias-Ceacero A, Lazo JS, and Roda-Navarro P (2020) Effect of Pharmacological Inhibition of the Catalytic Activity of Phosphatases of Regenerating Liver in Early T Cell Receptor Signaling Dynamics and IL-2 Production. *Int J Mol Sci* **21**:2530.

Behrens BC, Hamilton TC, Masuda H, Grotzinger KR, Whang-Peng J, Louie KG, Knutsen T, McKoy WM, Young RC, and Ozols RF (1987) Characterization of a cis-diamminedichloroplatinum(II)-resistant human ovarian cancer cell line and its use in evaluation of platinum analogues. *Cancer Res* **47**:414–418.

Chong PSY, Zhou J, Lim JSL, Hee YT, Chooi JY, Chung TH, Tan ZT, Zeng Q, Waller DD, Sebag M, et al. (2019) IL6 promotes a STAT3-PRL3 feedforward loop via SHP2 repression in multiple myeloma. *Cancer Res* **79**:4679–4688.

Cowley GS, Weir BA, Vazquez F, Tamayo P, Scott JA, Rusin S, East-Seletsky A, Ali LD, Gerath WF, Pantel SE, et al. (2014) Parallel genome-scale loss of function screens in 216 cancer cell lines for the identification of context-specific genetic dependencies [published correction appears in *Sci Data* (2014) 1:140044]. *Sci Data* **1**:140035.

Gottesman MM (2002) Mechanisms of cancer drug resistance. *Annu Rev Med* **53**:615–627.

Johnson SW, Ozols RF, and Hamilton TC (1993) Mechanisms of drug resistance in ovarian cancer. *Cancer* **71**(2, Suppl)644–649.

Lazo JS, Blanco IK, Tasker NR, Rastelli EJ, Burnett JC, Garrott SR, Hart DJ, McCloud RL, Hsu KL, Wipf P, et al. (2019) Next-generation cell-active inhibitors of the undrugged oncogenic PTP4A3 phosphatase. *J Pharmacol Exp Ther* **371**:652–662.

Lazo JS, Sharlow ER, Cornelison R, Hart DJ, Llaneza DC, Mendelson AJ, Rastelli EJ, Tasker NR, Landen Jr CN, and Wipf P (2021) Credentialing and pharmacologically targeting PTP4A3 phosphatase as a molecular target for ovarian cancer. *Biomolecules* **11**:969.

Lengyel E (2010) Ovarian cancer development and metastasis. *Am J Pathol* **177**: 1053–1064.

Liu H, Al-aidaroos AQ, Wang H, Guo K, Li J, Zhang HF, and Zeng Q (2013) PRL-3 suppresses c-Fos and integrin α2 expression in ovarian cancer cells. *BMC Cancer* **13**:80.

McQueeney KE, Salamoun JM, Ahn JG, Pekic P, Blanco IK, Struckman HL, Sharlow ER, Wipf P, and Lazo JS (2018) A chemical genetics approach identifies PTP4A3 as a regulator of colon cancer cell adhesion. *FASEB J* **32**:5661–5673.

McQueeney KE, Salamoun JM, Burnett JC, Barabutis N, Pekic P, Lewandowski SL, Llaneza DC, Cornelison R, Bai Y, Zhang ZY, et al. (2017) Targeting ovarian cancer and endothelium with an allosteric PTP4A3 phosphatase inhibitor. *Oncotarget* **9**:8223–8240.

Nilsson MB, Langley RR, and Fidler IJ (2005) Interleukin-6, secreted by human ovarian carcinoma cells, is a potent proangiogenic cytokine. *Cancer Res* **65**: 10794–10800.

Polato F, Codegoni A, Fruscio R, Perego P, Mangioni C, Saha S, Bardelli A, and Broggini M (2005) PRL-3 phosphatase is implicated in ovarian cancer growth. *Clin Cancer Res* **11**:6835–6839.

Rastelli EJ, Sannino S, Hart DJ, Sharlow ER, Lazo JS, Brodsky JL, and Wipf P (2021) Synthesis and evaluation of bifunctional PTP4A3 phosphatase inhibitors activating the ER stress pathway. *Bioorg Med Chem Lett* **46**:128167.

Rastelli EJ, Yue D, Millard C, and Wipf P (2021) 3D-Printed cartridge system for in-flow photo-oxygenation of 7-aminotheinopyridinones. *Tetrahedron* **79**:131875.

Reich R, Hadar S, and Davidson B (2011) Expression and clinical role of protein of regenerating liver (PRL) phosphatases in ovarian carcinoma. *Int J Mol Sci* **12**:1133–1145.

Ren T, Jiang B, Xing X, Dong B, Peng L, Meng L, Xu H, and Shou C (2009) Prognostic significance of phosphatase of regenerating liver-3 expression in ovarian cancer. *Pathol Oncol Res* **15**:555–560.

Salamoun JM, McQueeney KE, Patil K, Geib SJ, Sharlow ER, Lazo JS, and Wipf P (2016) Photooxygenation of an amino-thienopyridone yields a more potent PTP4A3 inhibitor. *Org Biomol Chem* **14**:6398–6402.

Shi Y, Xu S, Ngoi NYL, Zeng Q, and Ye Z (2021) PRL-3 dephosphorylates p38 MAPK to promote cell survival under stress. *Free Radic Biol Med* **177**:72–87.

Tasker NR, Rastelli EJ, Blanco IK, Burnett JC, Sharlow ER, Lazo JS, and Wipf P (2019) In-flow photooxygenation of aminothienopyridinones generates iminopyridinedione PTP4A3 phosphatase inhibitors. *Org Biomol Chem* **17**:2448–2466.

Thura M, Al-Aidaroos AQ, Gupta A, Chee CE, Lee SC, Hui KM, Li J, Guan YK, Yong WP, So J, et al. (2019) PRL3-zumab as an immunotherapy to inhibit tumors expressing PRL3 oncoprotein. *Nat Commun* **10**:2484.

Wagner EF and Nebreda AR (2009) Signal integration by JNK and p38 MAPK pathways in cancer development. *Nat Rev Cancer* **9**:537–549.

Wang Y, Zong X, Mitra S, Mitra AK, Matei D, and Nephew KP (2018) IL-6 mediates platinum-induced enrichment of ovarian cancer stem cells. *JCI Insight* **3**:e122360.

Wu CJ, Sundararajan V, Sheu BC, Huang RY-J, and Wei L-H (2019) Activation of STAT3 and STAT5 Signaling in Epithelial Ovarian Cancer Progression: Mechanism and Therapeutic Opportunity. *Cancers (Basel)* **12**:24.

Yang Y, Lian S, Meng L, Qu L, and Shou C (2017) Antibody array revealed PRL-3 affects protein phosphorylation and cytokine secretion. *PLoS One* **12**:e0169665.

Yu ZH and Zhang ZY (2018) Regulatory mechanisms and novel therapeutic targeting strategies for protein tyrosine phosphatases. *Chem Rev* **50**:122–129.

Yue J and López JM (2020) Understanding MAPK signaling pathways in apoptosis. *Int J Mol Sci* **21**:2346.

Address correspondence to: John S. Lazo, Department of Pharmacology, P.O. Box 80053, University of Virginia, Charlottesville, VA 22908-80053. E-mail: lazo@virginia.edu

JPET-AR-2022-001401. JS Lazo, KN Isbell, SA Vasa, DC Llaneza, EJ Rastelli, P Wipf, ER Sharlow. Disruption of ovarian cancer STAT3 and p38 signaling with a small molecule inhibitor of PTP4A3 phosphatase.

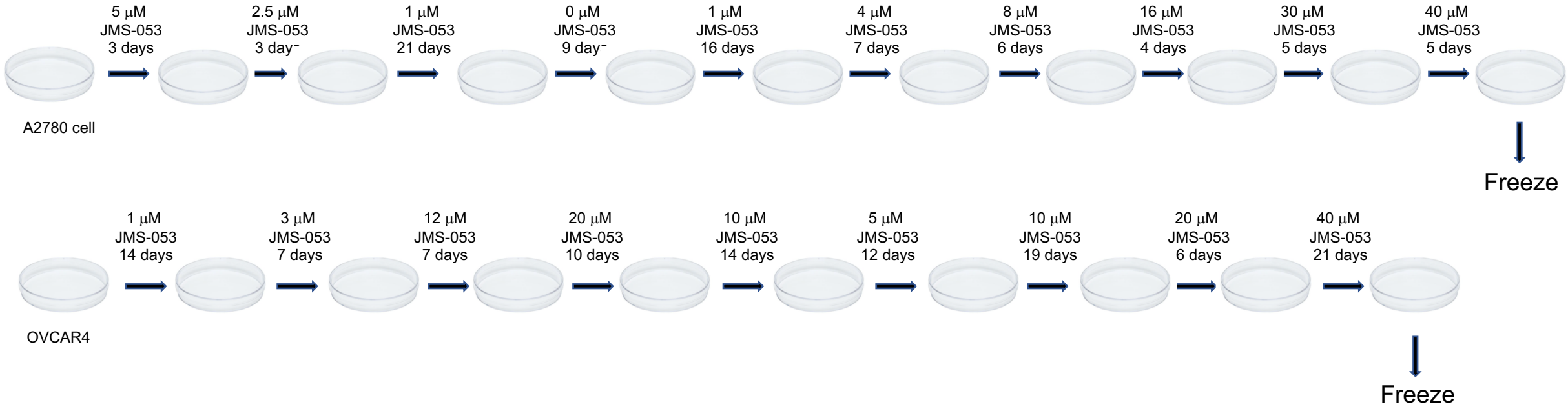

Supplemental Figure 1. Scheme for generating JMS-053 resistant cells. A2780 and OVCAR4 cells were initially exposed to 5 or 1 μM JMS-053, respectively. Cells were exposed to increasing or decreasing concentrations of JMS-053 as indicated. Ultimately, the resulting cells were exposed to 40 μM JMS-053 and then frozen for future use.

JPET-AR-2022-001401. JS Lazo, KN Isbell, SA Vasa, DC Llaneza, EJ Rastelli, P Wipf, ER Sharlow.
Disruption of ovarian cancer STAT3 and p38 signaling with a small molecule inhibitor of PTP4A3 phosphatase.

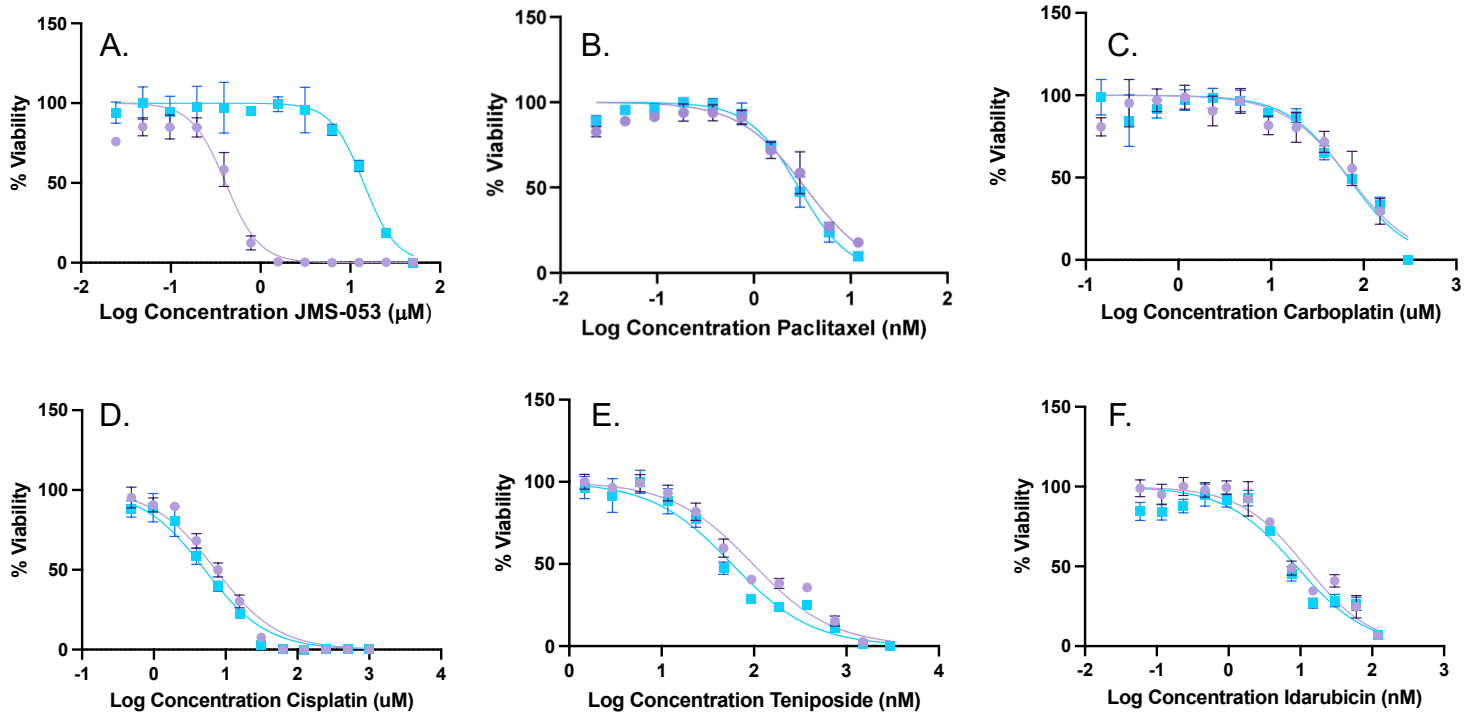

Supplemental Figure 2. Representative cytotoxicity curves with A2780 WT (purple) and A2780 RES (blue) cells. Bars=SD from 4 technical replicates.

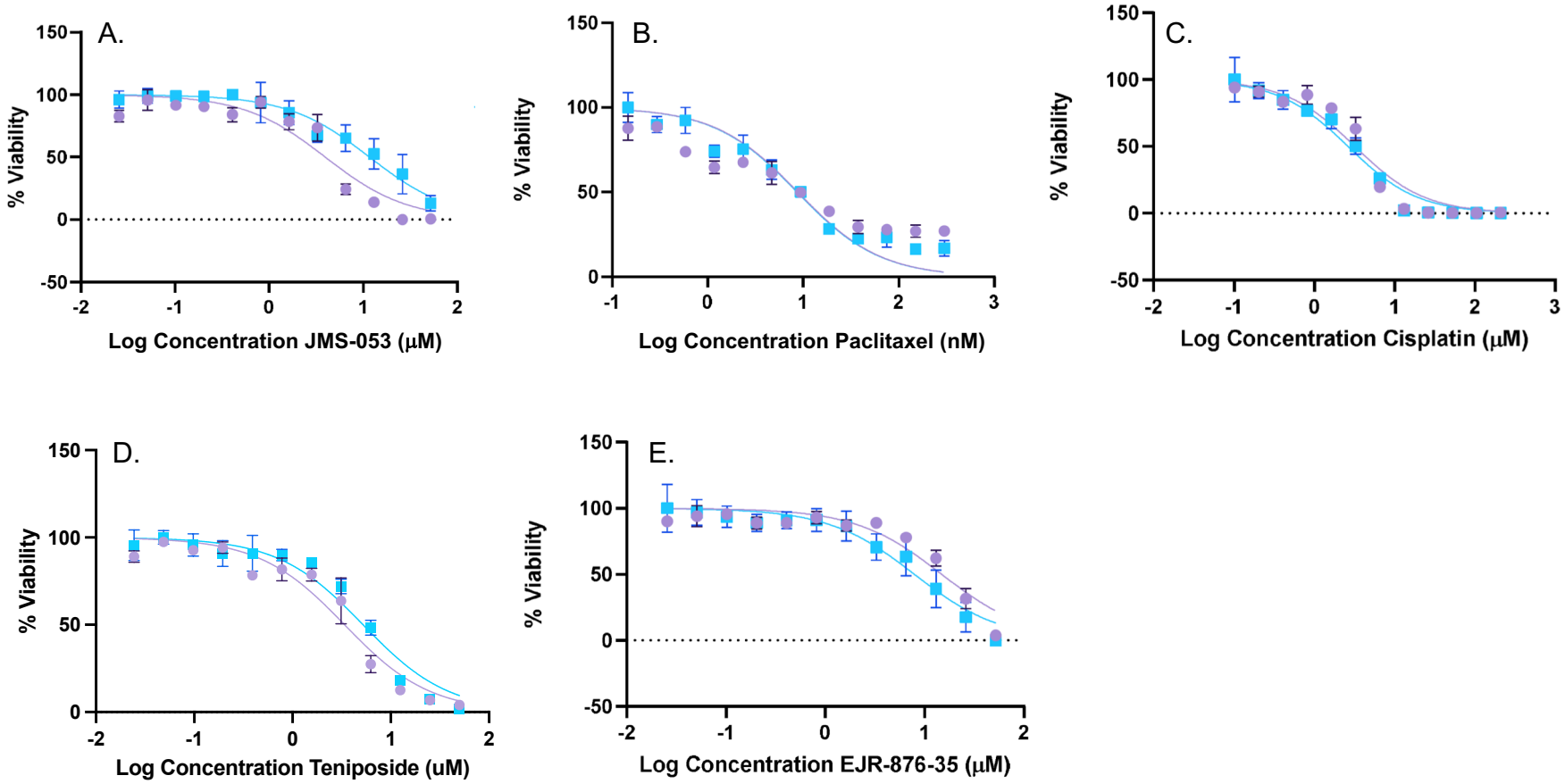

Supplemental Figure 3. Representative cytotoxicity curves with OVCAR4 WT (purple) and OVCAR4 RES (blue) cells. Bars=SD from 4 technical replicates.

JPET-AR-2022-001401. JS Lazo, KN Isbell, SA Vasa, DC Llaneza, EJ Rastelli, P Wipf, ER Sharlow. Disruption of ovarian cancer STAT3 and p38 signaling with a small molecule inhibitor of PTP4A3 phosphatase.

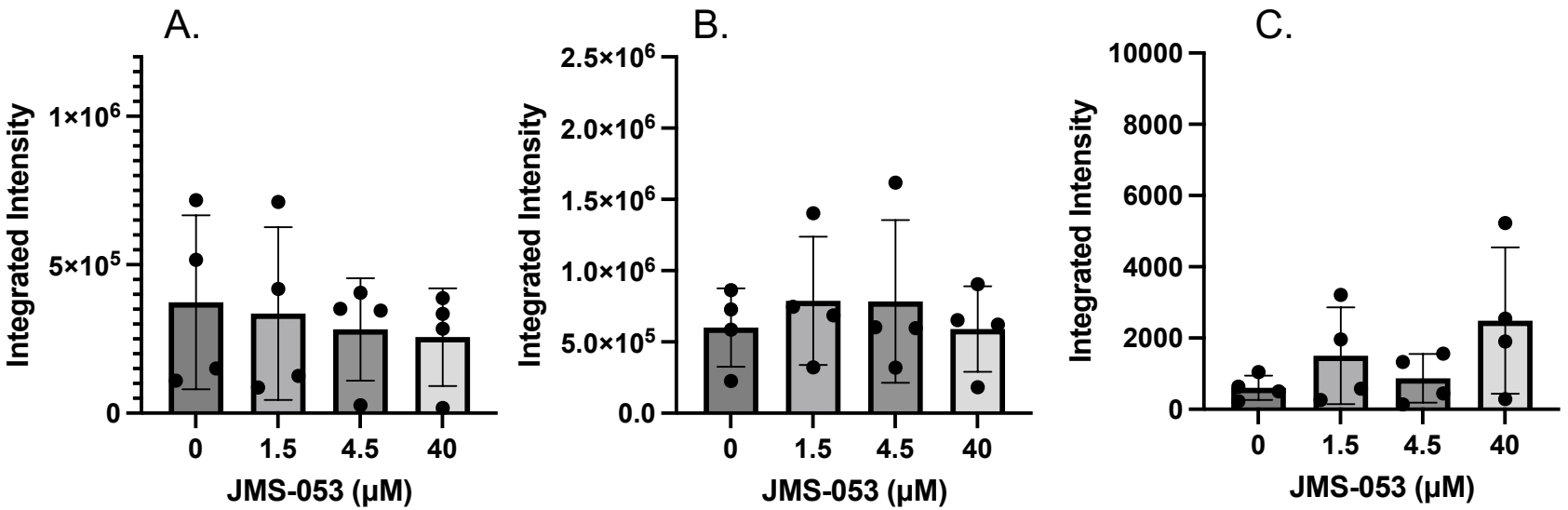

Supplemental Figure 4. Quantification of Western blots of total SHP-2 (**Panel A**), STAT5 (**Panel B**), and Y^{694} pSTAT5 (**Panel C**) in OVCAR4 cells 7 min after exposure to JMS-053. Each symbol is from an independent biological replicate. Bars=SD.

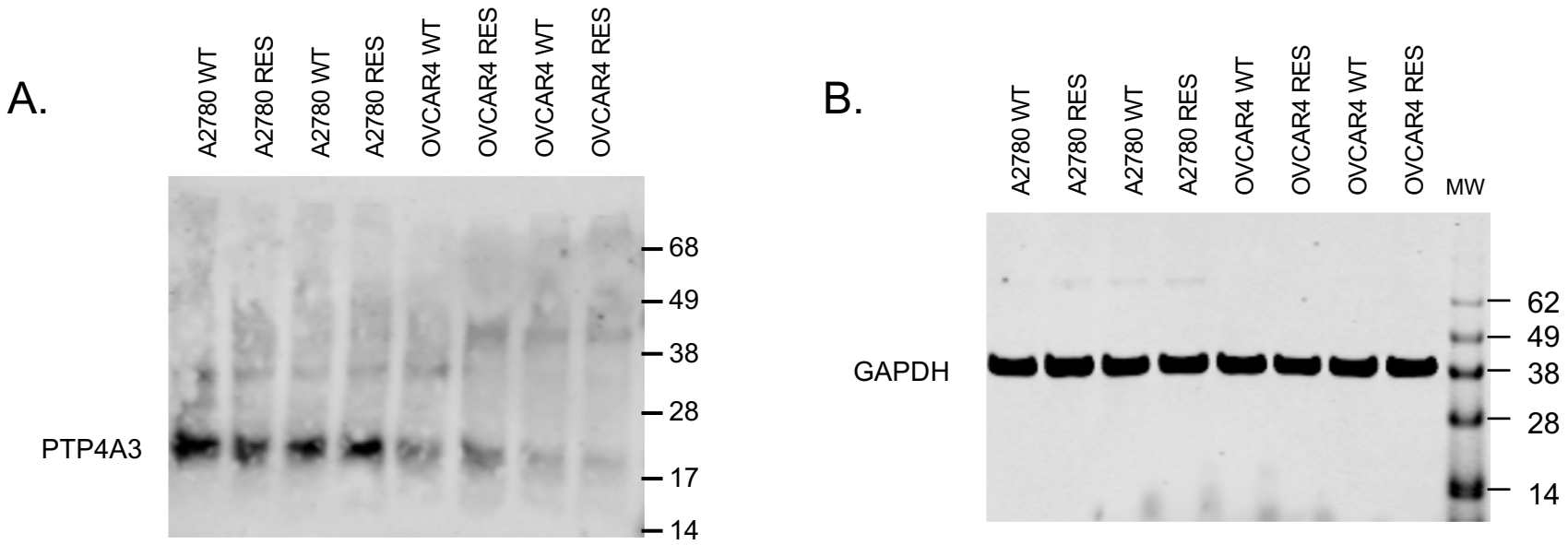

Supplemental Figure 5. Full Western blots used to compose Figure 3C. **Panel A.** PTP4A3. **Panel B.** GAPDH. MW are SeeBlue Plus2 (Thermo Fisher Scientific) molecular weight markers (kDa).

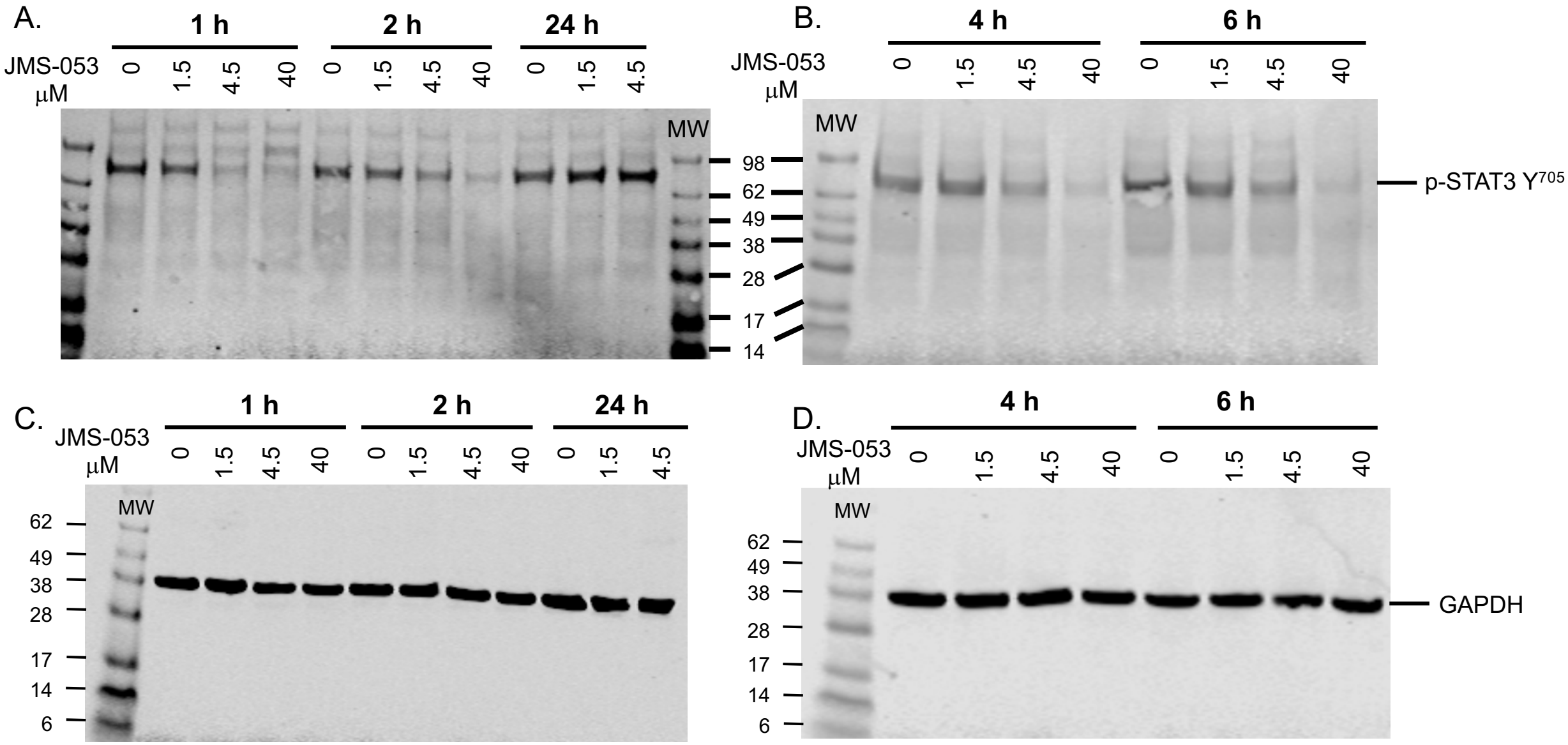

Supplemental Figure 6. Full Western blots used to compose p-STAT3 Y^{705} **(Panels A and B**) and GAPDH (**Panels C and D**) in Figure 5A. MW are SeeBlue Plus2 molecular weight markers (kDa) (Thermo Fisher Scientific).

Reagents and Antibodies

Drug	Supplier	Catalog Number	Lot Number
Teniposide	TCI America	T3109	7Z6MM-SF
Carboplatin	TCI America	C2043	MJ6DF-FL
Cisplatin	Selleckchem	S1166	S116615, S116616
Idarubicin	APExBIO	A2476	3
Paclitaxel	MedChem Express	HY-B00151/CS-1145	37434
KVX-053	AOBIOUS	AOB 31947	9041B

Antibody	Supplier	Catalog Number	Lot Number
PTP4A3	Novus Biologicals	MAB3219	WXH0419091, WXH0420091
GAPDH	Cell Signaling Technology	5174	8
Phospho-STAT3 (Y^{705})	Cell Signaling Technology	9131S	33, 43
Phospho-STAT3 (S^{727})	Invitrogen	MA5-33199	UL2896841
	Cell Signaling Technology	9134S	11
STAT3	Cell Signaling Technology	4904S	7
Phospho-SHP-2 (Y^{580})	Cell Signaling Technology	3703S	3
Phospho-SHP-2 (Y^{542})	Cell Signaling Technology	3751S	4
SHP-2	Cell Signaling Technology	3397S	5
Phospho-p38	Cell Signaling Technology	4511S	13
p38	Cell Signaling Technology	8690S	9
STAT5	Cell Signaling Technology	94205S	5
Phospho-STAT5 (Y^{694})	Cell Signaling Technology	4322S	8
Goat Anti-Rabbit IgG	Invitrogen	SA535571	UE282194
Goat Anti-Mouse IgG	Invitrogen	SA535521	UC282193

Supplemental Table 1. List of the suppliers, catalog number and lot number of reagents used in the study.